Kaon and Pion Production in Ni+Ni at 1, 1.4, and 1.9 AGeV

Dieter Best, GSI, for the FOPI collaboration

Institute for Physics and Nuclear Engineering, Bucharest
Central Research Institute for Physics, Budapest
Laboratoire de Physique Corpusculaire, Clermont-Ferrand
Gesellschaft für Schwerionenforschung, Darmstadt
Università and INFN, Florence
Physikalisches Institut der Universität Heidelberg, Heidelberg
Universität Mainz, Mainz
Institute for Experimental and Theoretical Physics, Moscow
Kurchatov Institute for Atomic Energy, Moscow
Forschungsinstitut Rossendorf, Dresden
Centre de Recherches Nucléaires and Université Louis Pasteur, Strasbourg
Institute of Experimental Physics, Warsaw University, Warsaw
Rudjer Boskovic Institute, Zagreb

Abstract

With phase II of the 4π–Detector at the SIS accelerator of GSI Darmstadt charged meson measurements became possible utilizing the particle identification capabilities of a central drift chamber and a Time–of–Flight Barrel. The system Ni+Ni has been investigated at the three incident energies 1930, 1450, and 1060 AMeV. The charged pion production has been measured in a large area of phase space and its dependence on collision geometry was analysed. In addition charged Kaons were identified. Delta resonances and Lambda particles were extracted by means of pion–proton correlations. The results are compared to earlier Streamer Chamber data from the Bevalac as well as to predictions of the dynamical model IQMD.

1 Introduction

In May 1994 the FOPI collaboration has performed an experiment with ^{58}Ni as projectile and target nucleus at three different incident energies: 1930, 1450, and 1060 AMeV, corresponding to 400, 310, and 240 AMeV CM energy, respectively.

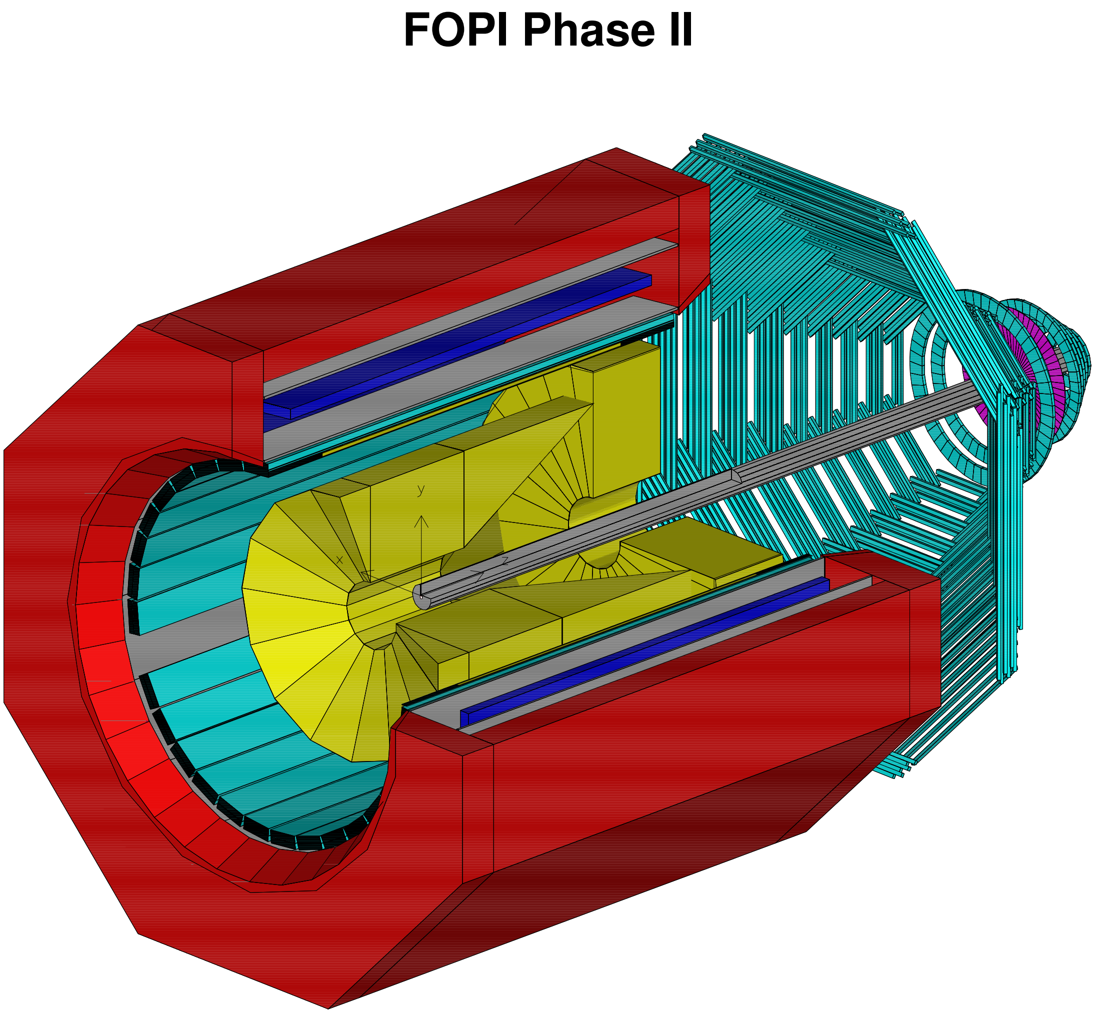

Figure 1: The FOPI detector at GSI.

One of the main goals of this experiment was the identification of strange particles, like K^+, and the measurement of the pion excitation function. Especially the Kaons are believed to be a useful messenger of the violent initial and perhaps very compressed and hot stage in the nuclear collision because of their relatively short mean free path. The measurement of the production cross section may yield another useful constraint for testing transport theories.

2 Experimental Setup

The FOPI detector [6], shown in figure 1, is a highly modular system of several subdetectors for fixed target experiments.
The detector was installed in three steps:
The main component of phase I is the highly segmented Forward Plastic Wall which

covers the polar angle between $1^o < \Theta_{Lab} < 30^o$ over the full azimuth. It provides ΔE and position information in addition to a Time–of–Flight (ToF) measurement. The Wall multiplicity is used to build a minimum bias and a central trigger (10 % of reaction cross section). This multiplicity measures the centrality of a heavy ion collision and its distribution is divided according to [5] in 5 multiplicity bins (PM1–PM5) in order to study the dependence of several observables on centrality.
Phase II completed the setup in 1992 by adding the Central Drift Chamber (CDC) as cylindrical tracking detector covering an additional range in polar angle of $30^0 < \Theta_{Lab} < 150^o$. The CDC is a jet chamber operating at atmospheric pressure and is similar to the DIOGENE drift chamber in Saclay [1].
The CDC provides for charged particles an accurate measurement of their r and ϕ coordinates via the recorded drift time ($\sigma_{r\phi}$ = 400 μm) and a less precise measurement of their z position along the beam axis by charge division (σ_z=10 cm). In addition it yields a multiple dE/dx measurement thus allowing particle identification by means of mean energy loss $< dE/dx >$ versus momentum p analysis. The relative energy resolution $\sigma(< dE/dx >)/< dE/dx >$ is about 20–30 %, the momentum resolution $\sigma(p)/p^2$ is about 1 %/GeV/c.
Pion, proton, deuteron, and triton identification is possible with the CDC alone using the Bethe–Bloch relation of the mean energy loss $< dE/dx >$ of a track with its momentum p. The high momentum limit of this method is overcome by adding the ToF information of the Barrel, thereby rising the particle identification capability. The chamber is surrounded by a ToF Plastic Barrel and a Cherenkov Barrel. Only a third of it has been installed during this experiment. The ToF resolution is about 1 ns FWHM.
Improvements in resolution are expected from progress in calibration.
The forward tracking chamber HELITRON will allow momentum measurements down to $\Theta_{Lab} \approx 7^o$. This detector was not used but will be commissioned together with the completed Barrel in the middle of 1995.
The tracking chambers as well as the Barrel operate inside a magnetic field of about 0.6 T of a Superconducting Solenoid which allows the momentum determination for charged particles.

3 Particle Identification

3.1 Kaon Identification

Plastic and Cherenkov Barrel do not supply sufficient information to define tracks. Hence CDC tracks have to be extrapolated to the Barrel strips. Then the Barrel hits are associated to those extrapolated tracks.
The direct measurement of the Time–of–Flight t with the Szintillator Barrel allows to calculate the particle mass from the momentum p and the path lenght L measured

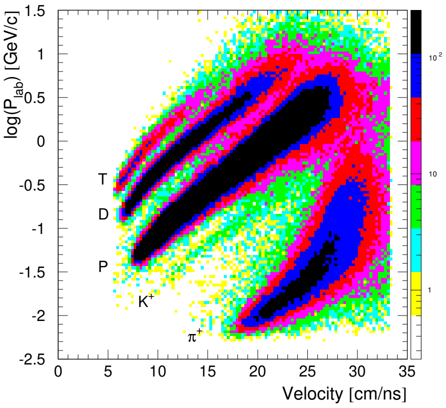

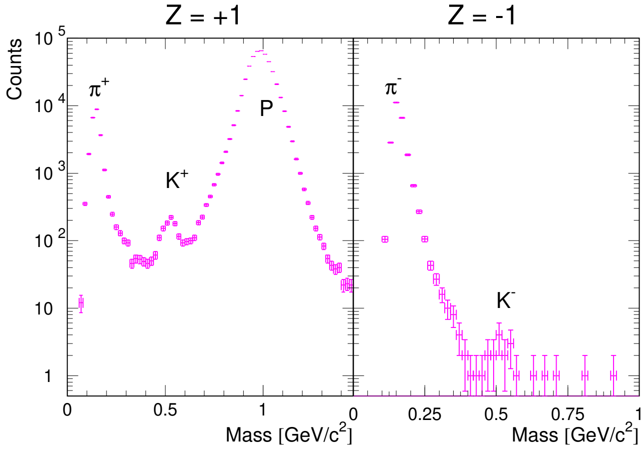

Figure 2: Momentum measured by the CDC plotted as function of velocity measured in the Barrel for particles with charge=+1.

Figure 3: Reconstructed mass using the matched CDC–Barrel data with $p_{Lab} < 600$ MeV/c for positively (a) and negatively charged particles (b).

with the CDC:

$$mc^2 = pc \cdot \sqrt{\left(\frac{ct}{L}\right)^2 - 1}.$$

By combining the momentum from the Central Drift Chamber (CDC) with the Time–of–Flight information of the Barrel figure 2 is obtained. Only positively charged particles are shown. Pions, protons, deuterons, and tritons are clearly resolved over the full velocity range. In addition a line between the pions and the protons is visible which is attributed to K^+ particles.

After linearizing this plot a mass spectrum is obtained as shown in figure 3. On the left hand side, between a peak at the pion mass and a much more pronounced proton peak another structure is clearly visible at the Kaon mass of 494 MeV.

The result of a corresponding analysis for negatively charged particles is presented on the right hand side. Besides the π^- peak another statistically significant peak is visible which can be attributed to the K^-. So far Kaons have been identified for the highest energy only.

However, the strength of the FOPI detector is the ability to measure a large area of phase space. In figure 4 a plot normalized transverse momentum $p_T^{(0)}/m$ ($p_T^{(0)}=p_T/(\beta\gamma)_{beam}$) versus scaled rapidity $y^{(0)}=y/y_{CM}-1$ is shown. The plot is affected by the acceptance of the Barrel which starts at a polar angle of 44^o. The upper momentum limit up to which K^+ particles can be identified is about 600 MeV/c at present. The lower momentum limit is about 100 MeV/c, since the K^+ particles need this minimum momentum in order to reach the Barrel.

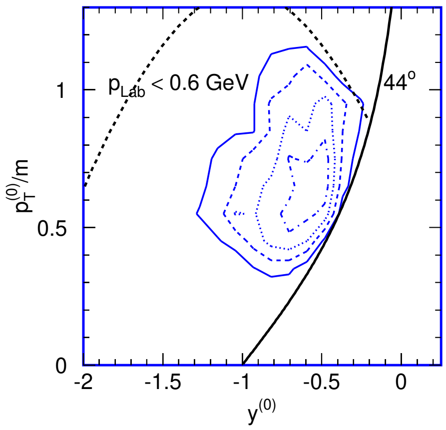

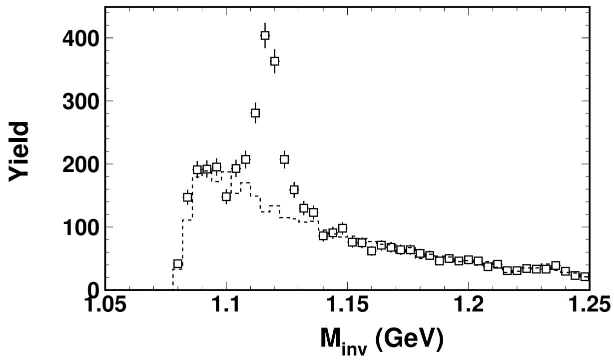

Figure 4: Scaled transverse momentum p$_T^{(0)}$ versus scaled rapidiy y$^{(0)}$ for K$^+$ particles measured in Ni+Ni collisions at 1930 AMeV.

Figure 5: Λ invariant mass spectrum for Ni+Ni collisions at 1930 AMeV. Squares show the full spectrum, the dashed line is the spectrum obtained by analysing mixed events.

3.2 Λ Identification

In order to conserve strangeness the K$^+$ is coproduced with another strange particle. The reaction channel which the lowest threshold, 1.6 GeV, is

$$N + p \longrightarrow N + \Lambda + K^+$$

In our measurement, the decay of the Λ in π^- and proton through weak interaction ($\Lambda \rightarrow p + \pi^-$, 64% branching ratio) was used for identification: This decay mode is identified by calculating the invariant mass of a (p,π^-) pair that intersects at a point (secondary vertex) outside the primary interaction region (primary vertex) compatible with cτ=7.89 cm of the Λ particle.
An invariant mass analysis, figure 5, shows a peak at the Λ position (m$_o$=1115 MeV) on top of combinatorial background. The dashed spectrum is obtained by analysing mixed events. The comparison of the two spectra shows that the combinatorial background is well controlled.

4 Δ Identification

The Ni+Ni data at 1930 AMeV show the presence of the Δ resonance in the final state.
An invariant mass analysis of (p,π^-) pairs coming from the target shows a strong correlation due to the Δ^o resonance, a corresponding analysis of (p,π^+) pairs shows the Δ^{++} resonance.

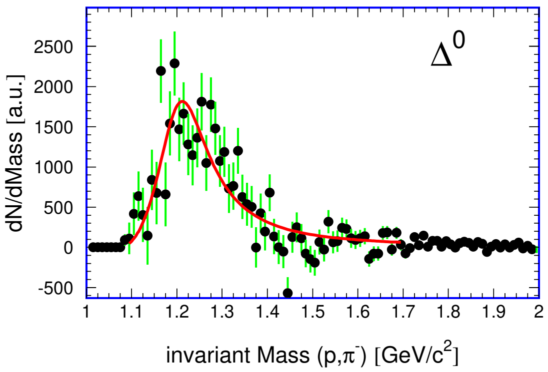

Figure 6: Extracted Δ^0 signal for Ni+Ni at 1930 AMeV.

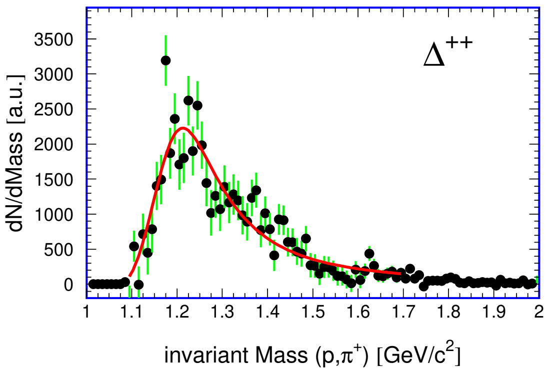

Figure 7: Extracted Δ^{++} signal for Ni+Ni at 1930 AMeV.

The peak position for both accessible Δ charge states appear to be close to the free Δ mass of about 1230 MeV. Compared to the free resonance a larger population of higher masses is observed, which can be parameterized by a larger effective width. The distribution has been fitted employing the parameterization given by Cugnon [4].
This result is consistent with earlier measurements which yield over a wide range of energy and system sizes resonance signals compatible with a free Δ [10].
However, this experimental result is not consistent with the expectation from the IQMD [9] model which shows a large shift of the Δ mass to lower masses. Further detailed studies are necessary.

5 Pion Production

5.1 Energy and Angular Distributions

Almost all pions measured are produced in Δ decays. As an example figure 8 shows the normalized transverse momentum p$_T^{(o)}$/m versus scaled rapidity y$^{(o)}$=y/y$_{CM}$-1 for π^- particles at the highest energy (1930 AMeV) and for semicentral events (PM3).
The 30^o line indicates where the acceptance of the CDC starts in polar angle. The lower momentum limit for pions is 70–100 MeV/c.
In addition the solid curves indicate the lines of constant energy of an isotropic source of negatively charged pions at midrapidity: It is clearly visible that the π^- distribution is incompatible with a single isotropic source.
In contrast to this kinetic energy spectra of these particles under an angle of 90^o in the CM system do not depend very much on centrality. Figure 9 shows this for the 1930 AMeV data and 5 different centrality bins (PM1–PM5).
The spectra are plotted on a logarithmic scale and divided by a factor $p \cdot E$ in order

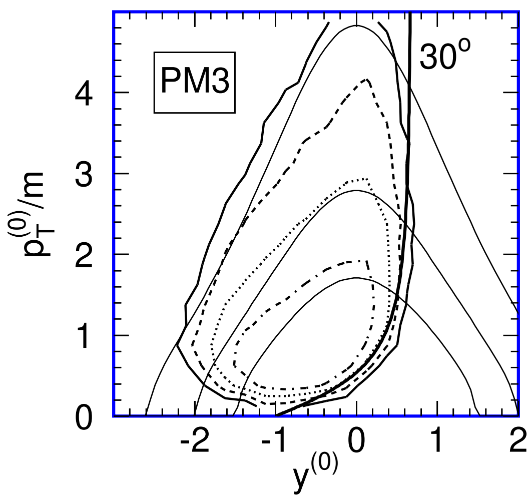

Figure 8: 1/p$_T$ dN/dp$_T$dy for negatively charged pions in Ni+Ni at 1930 AMeV and semicentral events (PM3). The data show a nonisotropic source around midrapidity.

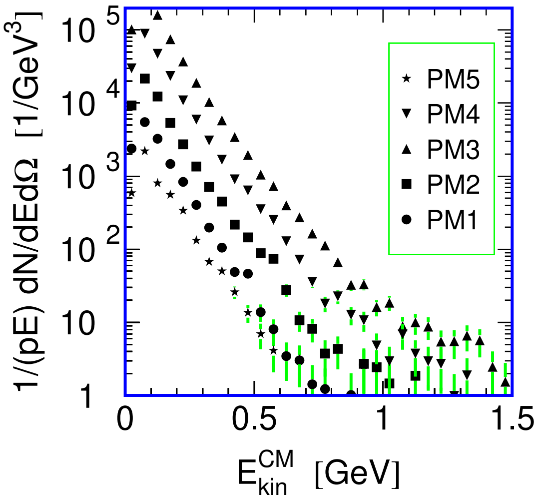

Figure 9: Energy spectra at Θ_{CM} = 90$^o\pm$10^o for negatively charged pions in Ni+Ni at 1930 AMeV and 5 different centrality bins.

to demonstrate the deviation from an exponential fall off of a thermal distribution. The spectrum shape is approximately exponential,

$$\frac{1}{pE}\frac{dN}{dEd\Omega} \approx \exp(-E_{\pi}^{CM}/E_o),$$

for all energies and polar angles. The slope parameters E$_o$ determined between E$_{kin}^{cm}$=100 MeV and 600 MeV are the same within the error bars for all centrality bins.

5.2 Excitation Function and Multiplicities

Figure 10 shows the total pion multiplicity $N(\pi)$ as a function of the participant nucleons N_{part} for Ni+Ni at the three incident energies. Except for the highest energy it is a linear function for each incident energy. The errors reflect the precision of the mean and are mostly smaller than the marker size. Systematic errors from the track reconstruction algorithms [3] due to limited drift chamber resolution and imperfect calibration are under investigation.
The number of participants was derived from the track multiplicity of the outer Plastic Wall. In the geometrical model a certain cross section σ corresponds to a certain impact parameter *b*. From this quantity N_{part} was derived using the formula from [7].
The total pion multiplicity was obtained from the isobar model [11]. With this model

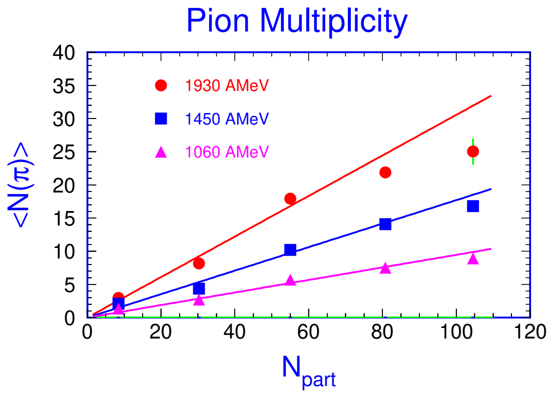

Figure 10: The mean pion multiplicity as a function of the number of participant nucleons N_{part} in the Ni+Ni reactions at three incident laboratory energies. The lines are straight line fits (y=ax) to the data.

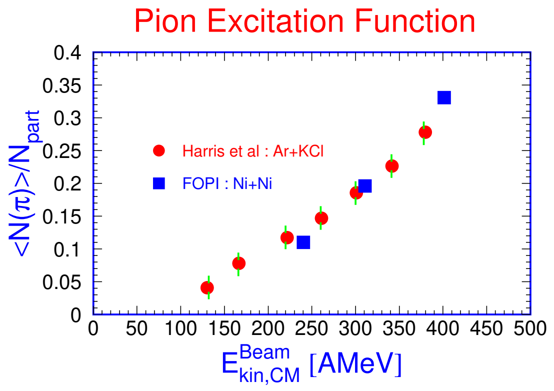

Figure 11: Excitation function of $< N(\pi) > / N_{part}$ for almost equal–mass collisions. Circles were obtained with a streamer chamber for high–multiplicity events in Ar+KCl collisions [8], whereas squares are obtained with the FOPI jet chamber.

the following pion ratios are determined:

$$\begin{aligned} < N(\pi^-) > / < N(\pi^0) > / < N(\pi^+) > &= \\ (5N^2 + NZ)/(N^2 + 4NZ + Z^2)/(5Z^2 + NZ) &= 1.12/1.06/1 \end{aligned}$$

The calculated ratio $< N(\pi^-) > / < N(\pi^+) >$ is in agreement with the data at all three incident energies in the momentum range 70 MeV/c up to 600 MeV/c where the π^+ particles can be unambigiously identified with a mean energy loss $< dE/dx >$ versus momentum analysis of the CDC data alone. Therefore only π^- particles with $y_{CM} < 0$ are used. This number is multiplied by 2 in order to get an estimate of the 4π multiplicity. Via the isobar ratios the 4π multiplicities of π^o and π^+ particles and thus the total pion multiplicity are obtained.
This was done in order to get a comparison with data from [8], where the excitation function of negatively charged pions with Ar+KCl and La+La was measured using a streamer chamber device with full geometrical acceptance. The data were analysed with a scanning film technique and no dependence on the system mass was found. From the negative pion multiplicity the total pion multiplicity was extrapolated.
Figure 11 shows the pion excitation function as obtained from [8] with Ar+KCl at 132, 166, 220, 260, 300, 341, and 378 AMeV CM energy compared to the FOPI results from Ni+Ni. The two datasets are compatible within the error bars. The errors of the FOPI data are pure fit errors and smaller than the symbol size. However, more detailed efficiency studies are still necessary and under way.
Up to now only for the 1060 AMeV data model calculations are available. The IQMD model [2] overestimates the experimental pion multiplicities by a factor of

about two.

6 Summary and Outlook

In summary, we have shown that Kaons, Lambdas and Deltas have been successfully identified with the FOPI 4π device for the highest energy data, 1.93 AGeV, in a large area of phase space.
K^+ as well as K^- particles are identified by combining the tracks of the CDC with the ToF measurement of the Barrel, whereas Λ and Δ particles are identified with the CDC alone by means of an invariant mass analysis.
Pions have been analysed for all available energies (1.06, 1.45, 1.93 AGeV). The existence of a nonisotropic pion source at midrapidity could be shown. The slope of the dominant component in the kinetic energy specta does not depend significantly on centrality. The Pion excitation function is compatible with BEVALAC data.
K^+ data have been presented for the highest energy data (1.93 AGeV) only. In one of the next steps a more detailed analysis of the 1.06 and 1.45 AGeV data will study real subthreshold Kaon production and a Kaon excitation function could be obtained.
One of the key issues is Kaon flow. A rough analysis has shown that the K^+ emission with respect to the reaction plane is isotropic. In a first analysis preliminary ratios K^+/π^+ and Λ/π^+ have been determined, and their dependence on centrality has been studied. These results are very preliminary, however, since carefull efficiency studies are necessary.
An extended analysis of (K,π) correlations could reveal K^* particles, correlating (π^+,π^-) pairs the K^o, and (K^+,K^-) invariant mass analyses the Φ Meson which is expected to be a sensitive probe of in medium effects.

7 Acknowledgements

The author wants to thank Martin Trzaska for providing the histograms for the Δ particle, Norbert Herrmann for the pictures concerning the Λ baryon, and James Ritman for the Kaon identification plots.

References

[1] J. P. Alard et al., *NIM*, A261 (1987) 379–398.

[2] S. Bass, Master's thesis, Universität Frankfurt, 1993.

[3] D. Best, Master's thesis, Universität Mainz, 1992.

[4] J. Cugnon and M. C. Lemaire, *Nucl. Phys.*, A489 (1988) 781.

[5] K. G. R. Doss et al., *PRL*, 59 (1987) 2720.

[6] A. Gobbi et al., *NIM*, A324 (1993) 156–176.

[7] J. Gosset et al., *Phys. Rev.*, C16 (1977) 629.

[8] J. W. Harris et al., *PRL*, 58 (1987) 463.

[9] C. Hartnack et al. *Phys. Lett.*, B336 (1994) 131.

[10] T. K. Hemmik, *Nucl. Phys.*, A566 (1994) 435c.

[11] R. Stock, *Phys. Rep.*, 135 (1986) 259–315.